

Received March 4, 2020, accepted March 16, 2020, date of publication March 20, 2020, date of current version April 7, 2020.

Digital Object Identifier 10.1109/ACCESS.2020.2982366

Investigate Contribution of Multi-Microseismic Data to Rockburst Risk Prediction Using Support Vector Machine With Genetic Algorithm

BING JI¹, FA XIE¹, XINPEI WANG¹, SHENQUAN HE², AND DAZHAO SONG²

¹School of Control Science and Engineering, Shandong University, Jinan 250061, China

²School of Civil and Resources Engineering, University of Science and Technology Beijing, Beijing 100083, China

Corresponding author: Xinpei Wang (wangxinpei@sdu.edu.cn)

This work was supported in part by the National Key Research and Development Program of China under Grant 2018YFB1305400, and in part by the National Natural Science Foundation of China under Grant 61673246.

ABSTRACT As a severe hazard in coal mining and rock excavation, the rockburst is usually induced by the high energy tremor. Microseismic (MS) monitoring is suggested to forecast the rockburst risk to reduce its damage. The paper aims to investigate contribution of multi-MS data, including MS raw wave data and MS energy data, to prediction of the high energy tremor, using support vector machine (SVM) together with genetic algorithm (GA). MS monitoring data recorded for more than 400 days at Wudong coal mine of Xinjiang, China, were used in the paper. 132 and 24 features are initially extracted from MS raw wave and energy data in the frequency domain, entropy and time-frequency domain, respectively. GA is not only used to select effective ones among initially extracted features, but also optimize hyperparameters for SVM to classify high energy tremors from general MS events. The performances of the proposed approach based on multi-MS data are evaluated by cross-validation. The results show that the classifier achieves 98% sensitivity, 88% accuracy and 87% specificity using both MS raw wave and energy data, which is better than solely utilizing MS raw wave (98% sensitivity, 84% accuracy and 83% specificity) or energy data (98% sensitivity, 86% accuracy and 85% specificity). These findings suggest that MS raw wave data makes important contribution to rockburst risk prediction as well as MS energy data, and the better performance can be achieved when utilizing two kinds of data simultaneously.

INDEX TERMS Rockburst risk prediction, microseismic monitoring, microseismic raw wave data, support vector machine, genetic algorithm.


I. INTRODUCTION

A rockburst refers to a violent fracture of rock occurring in coal mining or rock excavation with a sudden release of accumulated strain energy [1]. The pressure on adjacent rocks is significantly reduced due to coal mining or rock excavation, which potentially leads to rockburst. The risk of rockburst rises, as mining depth and intensity of coal resources increase.

As a severe hazard, the rockburst leads to serious destruction to mine equipment and buildings in mining areas [2]–[6]. According to the statistics, 169 coalmine accidents occurred with 211 deaths in China from January to August in 2018 [7]. Five workers lost their lives by mining accidents in Australia on 20 December 2018 [8]. Twelve coal fatalities happened in

the USA in 2018 [9]. A serious rockburst accident occurred in Hongyang No. 3 Coal Mine of Shenyang Coking Coal Co., Ltd. on 11 November 2017, which caused ten workers killed and one worker injured [10]. A rockburst occurred in Longyun Coal Industry Co., Ltd. on 20 October 2018, causing different degrees of damage to the roadway within approximately 100 meters and 21 deaths [11].

In order to reduce rockburst damage, several methods were proposed to predict the probability and potential areas of the rockburst, including MS monitoring techniques, acoustic emission, electromagnetic radiation, stress monitoring and drilling cutting [12]–[20]. The engineering requirements for stress monitoring and drilling cutting are very high, resulting in high costs, discontinuous monitoring and limited range. They are usually used as auxiliary monitoring methods for early warning of rockburst risk. Electromagnetic radiation is

The associate editor coordinating the review of this manuscript and approving it for publication was Hao Luo .

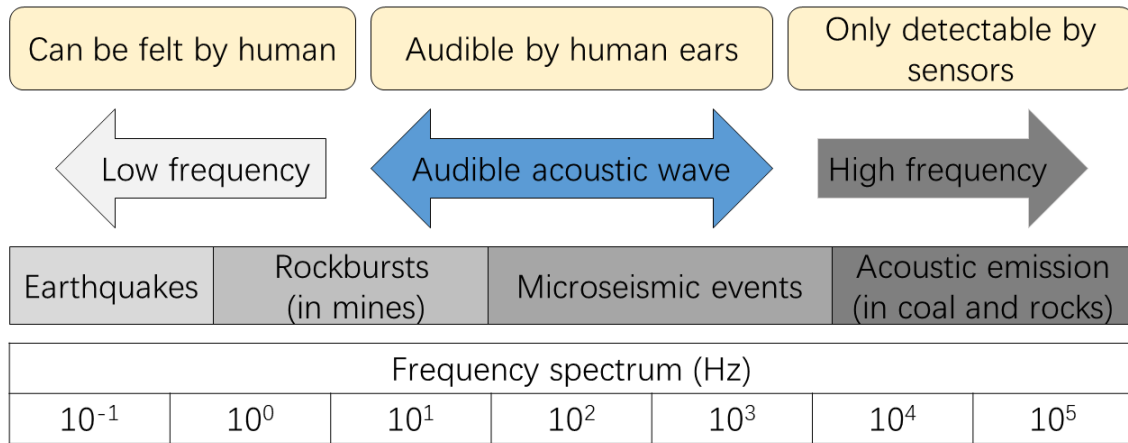


FIGURE 1. Frequency characteristics of seismic motion wave (modified according to [21]).

mainly utilized for partial monitoring, since its monitoring range is limited, and always influenced by the operation of cables and equipments. The acoustic emissions technique monitors low-energy and high-frequency signals with a small monitoring range and weak anti-interference ability, while MS monitoring can monitor events with a wide monitoring range and strong anti-interference ability, as shown in Fig. 1 [21], [22].

MS monitoring analyses the precursor characteristics of the rockburst by observing micro-fractures, resulted from local damage inside the rock mass under the external force disturbance [23], [24]. The MS monitoring technique has several advantages, including without effect on production activities, and monitoring MS events of the whole mining area in real-time [25]. A group of studies were performed to forecast the rockburst based on MS monitoring, and indeed obtained many useful findings [26], [27]. MS waves before the rockburst were investigated, suggesting that characteristics of the wave’s velocity, amplitude, and frequency as well as rock stress state can be used for the rockburst warning [28]–[36]. The relationship between MS waves and the rockburst was analysed, indicating the features extracted from MS waves together with rock stress can be utilized to predict rockburst [25], [37]–[41].

Although great potentials of MS monitoring have been demonstrated as discussed above, as far as we know, these studies mainly used MS energy data to predict the rockburst, but failing to utilize MS raw wave data. In this context, this paper aims to investigate contribution of MS raw wave and energy data to rockburst risk prediction. In this paper, a high energy tremor is defined as a MS event with a sudden release of energy greater than 1×10^6 J. High energy tremors usually cause obvious vibration in a certain area of underground mine, accompanied by the drop of small coal and rock blocks, which seriously threatens workers’ safety. Furthermore the high energy tremor can even induce severe rockburst disasters under certain circumstances. Therefore, early warning of the high energy tremor is of great significance to rockburst risk prediction.

MS monitoring data continuously recorded for more than 400 days at the Wudong coal mine of Xinjiang, China, were used in the paper. 132 and 24 features are initially extracted from MS raw wave and energy data in the frequency domain, entropy and time-frequency domain, respectively. Although MS data over 400 days were collected, the number of high energy tremors is limited. Therefore, this is a typical high-dimensional small samples issue. Support vector machine (SVM) is a machine learning method based on statistical learning theory [42] and the structural risk minimization principle [43], having advantages to solve small sample, nonlinear and high-dimensional pattern recognition problems [44]. Meanwhile genetic algorithm (GA) is a group intelligent optimization algorithm based on natural selection and evolution, and can seek global optimal solutions without any initialization information [45]. Considering the advantages of SVM and GA, a GA-SVM based approach is proposed to analyse multi-MS data. Specifically, GA is used to select effective ones from 156 features and optimize hyperparameters of the SVM classifier. SVM classifies high energy tremors from general MS events based on features selected by GA. The performances of the approach are evaluated by cross-validation. It should be noted that the key point of this paper is to demonstrate advantages of extracting a variety of features from both MS raw wave and energy data in frequency domain, entropy and time-frequency domain, and further investigate contribution of MS raw wave and energy data in rockburst risk prediction.

II. MS DATA DESCRIPTION

External force is able to lead to micro-fractures inside the rock mass. Such micro-fractures can be regarded as a MS event, and detected by the MS monitoring system. Data from the monitoring system records time, energy and coordinates of the MS event. In this work, MS data are obtained by ARAMIS M/E MS Monitoring System (the system is developed by EMAG Industrial Technology Innovation Institute of Poland; detailed information regarding this system is available at <http://www.cttemag.pl/en>) in Wudong coal

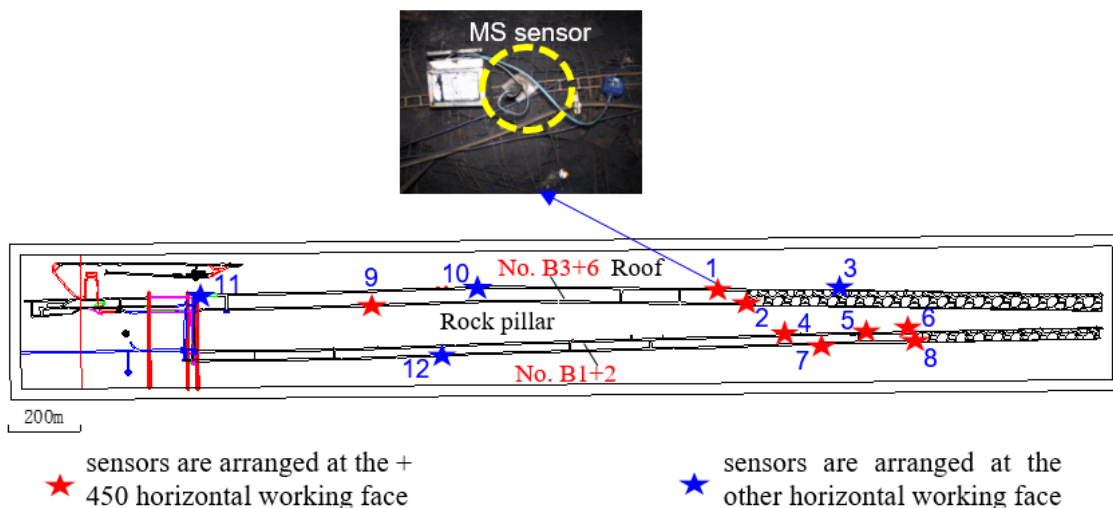


FIGURE 2. Sketch of the layout of the MS system in Wudong coal mine (modified according to [56]).

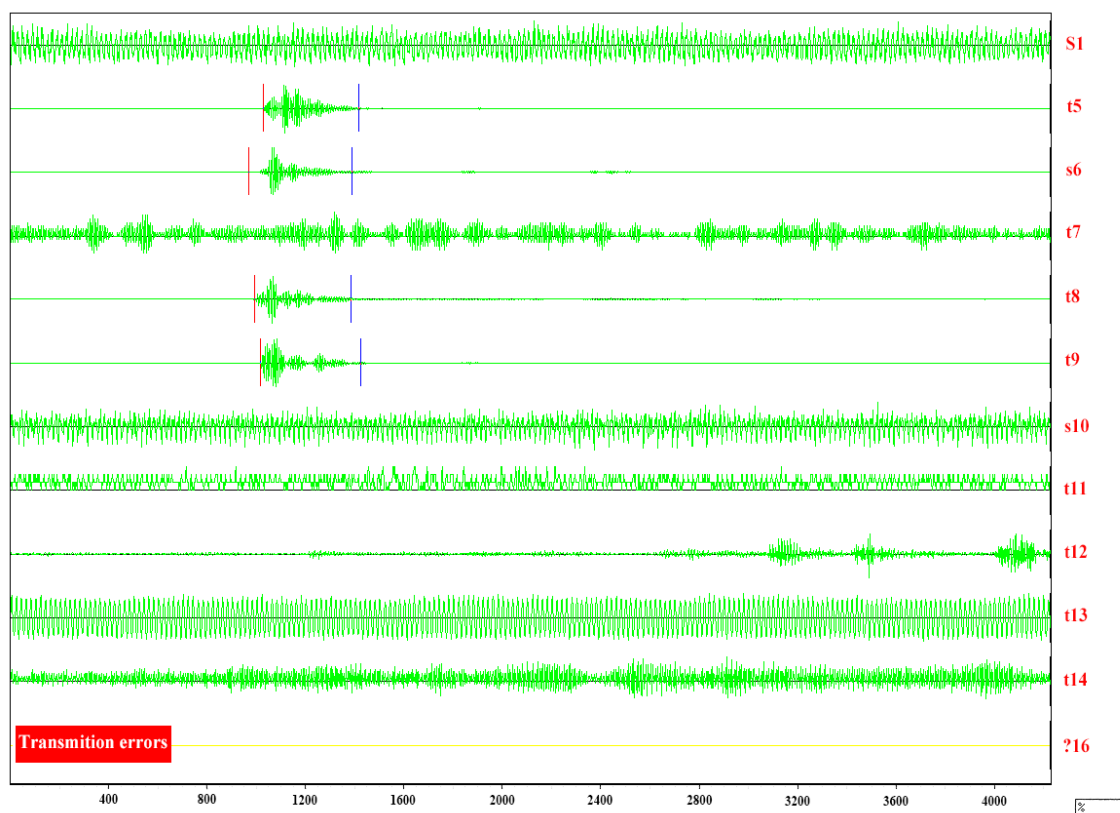


FIGURE 3. The raw wave signal (including the interference signal) of a MS event detected by MS sensors.

mine, Xinjiang, China. The MS sensor distribution of the MS monitoring system is shown in Fig. 2. When a MS event occurs, the MS monitoring system can detect a significant MS waveform in multiple channels (one channel corresponds to a MS sensor). MS monitoring data from June 6, 2016 to March 22, 2018 are collected.

MS data includes MS raw wave and energy data. Fig. 3 shows a raw wave signal (including the interference

signal) of a MS event detected by MS sensors of the monitoring system during a certain period, for example. Table 1 lists MS energy data calculated by the monitoring system using MS raw wave data of ten MS events. As shown in Table 1, the data includes time, source coordinates, energy and other information of MS events.

The high energy tremor is likely to induce severe rockburst hazards, this paper aims to analyse the MS data before the

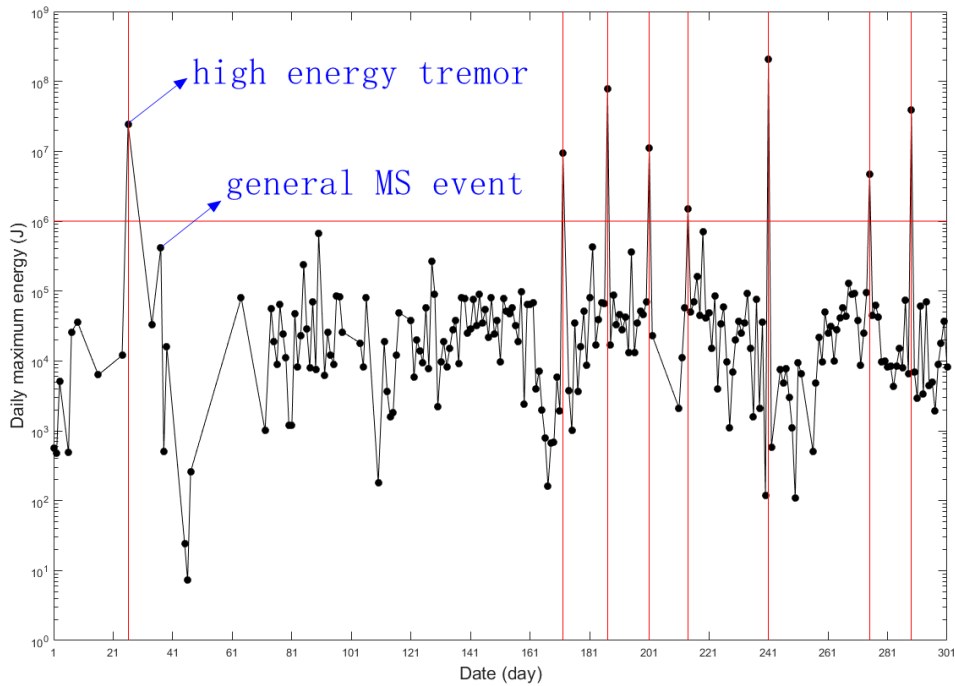


FIGURE 4. MS daily maximum energy.

TABLE 1. Ten MS events and related information of time, source coordinates and energy.

| No. | Date | Time | X | Y | Z | Energy (J) |
|-----|----------|----------|------|------|-----|------------|
| 1 | 2018/1/4 | 0:36:38 | 1478 | 4575 | 459 | 220 |
| 2 | 2018/1/4 | 0:37:03 | 1462 | 4597 | 454 | 0.7 |
| 3 | 2018/1/4 | 1:28:59 | 1446 | 4541 | 459 | 13 |
| 4 | 2018/1/4 | 2:42:56 | 1545 | 4541 | 454 | 80 |
| 5 | 2018/1/4 | 3:51:22 | 1504 | 4519 | 459 | 1200 |
| 6 | 2018/1/4 | 12:51:19 | 1286 | 4517 | 459 | 37 |
| 7 | 2018/1/4 | 18:19:07 | 1555 | 4597 | 454 | 94000 |
| 8 | 2018/1/4 | 20:12:21 | 1446 | 4519 | 459 | 54 |
| 9 | 2018/1/5 | 2:32:03 | 1529 | 4597 | 454 | 150 |
| 10 | 2018/1/5 | 3:01:58 | 1520 | 4519 | 459 | 160 |

occurrence of high energy tremors, and predict the occurrence of high energy tremors. The MS energy data directly obtained from the MS monitoring system (Table 1) are processed to obtain the daily maximum energy and the daily total energy of the MS event. The high energy tremor is marked according to the daily maximum energy value. Fig. 4 presents a graph of daily maximum energy as a function of date. The abscissa and ordinate represent the date and daily maximum energy value in logarithms respectively. The high energy tremor is marked with a red vertical line.

III. METHODOLOGY

A approach combining SVM with GA is proposed to analyse MS energy data or/and MS raw wave data in this paper, which aims to predict the high energy tremor based on previous MS data. As demonstrated in Fig. 5, the proposed approach contains the following steps: feature extraction, feature selection and hyperparameters optimization based on GA, and SVM model construction.

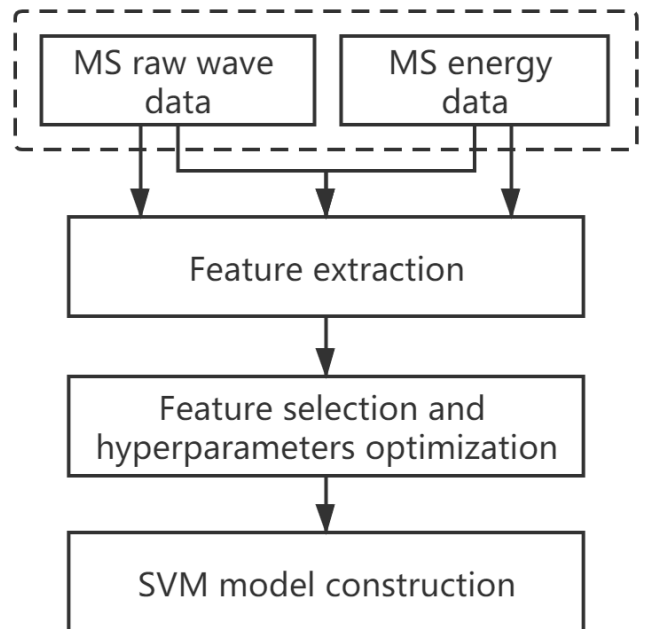


FIGURE 5. Flow diagram of the proposed approach.

A. FEATURE EXTRACTION

MS raw wave and energy data are used to extract potential features for predicting high energy tremors in this paper. To be specific, the comprehensive statistical features are extracted from MS raw wave data in the frequency domain, while entropy and time-frequency domain features are extracted from MS energy data (MS energy data contains daily maximum energy and daily total energy).

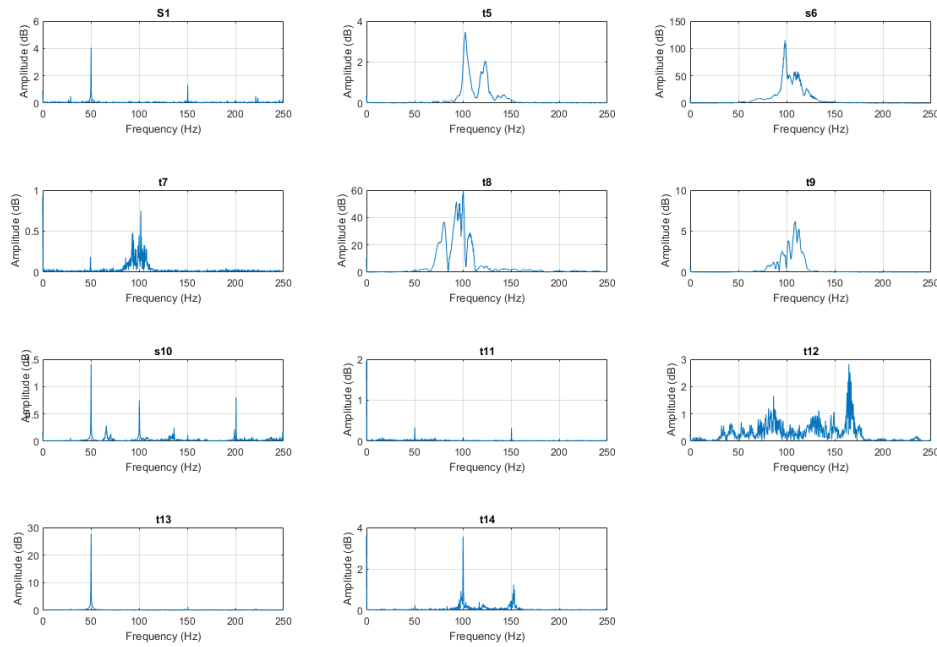


FIGURE 6. An example of FFT of the raw wave data sequence of each channel of the MS event shown in Fig. 3.

1) FREQUENCY DOMAIN-BASED COMPREHENSIVE STATISTICAL FEATURES OF MS RAW WAVE DATA (12 × 11.132 FEATURES)

The frequency spectrum [39] is estimated for the raw wave data from all channels in each MS event using discrete Fourier transform. Fig. 6 illustrates the frequency spectrum of raw wave data shown in Fig. 3. The proportions of the high-frequency and low-frequency components in spectrums are obtained according to thresholds from 50 to 150 Hz with a 10 Hz interval. For each MS event, mean and maximum values of high-low frequency ratios of all channels are then calculated. For all MS events in one day, the sum, mean, variance, median, maximum, and minimum values of the above mean and maximum values are calculated as features of MS raw wave data, respectively. The features and descriptions are listed in Table 2. Finally, envelopes are calculated for these 132 value sequences with a window length of thirteen days, since the shortest time interval for the marked high energy tremor is thirteen days.

2) ENTROPY FEATURES OF MS ENERGY DATA (2 × 3 × 2 = 12 FEATURES)

The sample entropy (SampEn) reflects the complexity of signals by measuring the probability of generating a new pattern in signals. It can be used to identify the same pattern in the time series [46]. Envelope, sliding average and sliding variance are calculated for the daily maximum energy sequence and daily total energy sequence. The sliding window width is set to thirteen days (consistent with that of the features extracted from MS raw wave data) with the sliding step of one day. Then, the SampEn and quadratic SampEn (the def-

TABLE 2. Overview of frequency domain-based comprehensive statistical features of MS raw wave data.

| Feature index | Feature name | Physical meaning |
|---------------|-----------------|---|
| 1-11 | s_mean_ratio | Sum of the mean value of the amplitude ratio of the high and low frequency spectrum for each day |
| 12-22 | mean_mean_ratio | Mean of the mean value of the amplitude ratio of the high and low frequency spectrum for each day |
| 23-33 | var_mean_ratio | Variance of the mean value of the amplitude ratio of the high and low frequency spectrum for each day |
| 34-44 | med_mean_ratio | Median of the mean value of the amplitude ratio of the high and low frequency spectrum for each day |
| 45-55 | max_mean_ratio | Maximum of the mean value of the amplitude ratio of the high and low frequency spectrum for each day |
| 56-66 | min_mean_ratio | Minimum of the mean value of the amplitude ratio of the high and low frequency spectrum for each day |
| 67-77 | s_max_ratio | Sum of the maximum value of the amplitude ratio of the high and low frequency spectrum for each day |
| 78-88 | mean_max_ratio | Mean of the maximum value of the amplitude ratio of the high and low frequency spectrum for each day |
| 89-99 | var_max_ratio | Variance of the maximum value of the amplitude ratio of the high and low frequency spectrum in each day |
| 100-110 | med_max_ratio | Median of the maximum value of the amplitude ratio of the high and low frequency spectrum in each day |
| 111-121 | max_max_ratio | Maximum of the maximum value of the amplitude ratio of the high and low frequency spectrum in each day |
| 122-132 | min_max_ratio | Minimum of the maximum value of the amplitude ratio of the high and low frequency spectrum in each day |

inition of quadratic SampEn is included in Appendix A) are calculated for the envelope, the sliding average and the sliding variance as features, respectively. The details of calculating SampEn can be found in the work of Zhao *et al.* [46].

TABLE 3. Overview of the entropy features of MS energy data.

| Feature index | Feature name | Physical meaning |
|---------------|--------------|---|
| 1 | SE_env_max | SampEn of envelope of daily maximum energy |
| 2 | QSE_env_max | Quadratic SampEn of envelope of daily maximum energy |
| 3 | SE_ave_max | SampEn of sliding average of daily maximum energy |
| 4 | QSE_ave_max | Quadratic SampEn of sliding average of daily maximum energy |
| 5 | SE_var_max | SampEn of sliding variance of daily maximum energy |
| 6 | QSE_var_max | Quadratic SampEn of sliding variance of daily maximum energy |
| 7 | SE_env_cum | SampEn of envelope of daily cumulative energy |
| 8 | QSE_env_cum | Quadratic SampEn of envelope of daily cumulative energy |
| 9 | SE_ave_cum | SampEn of sliding average of daily cumulative energy |
| 10 | QSE_ave_cum | Quadratic SampEn of sliding average of daily cumulative energy |
| 11 | SE_var_cum | SampEn of sliding variance of daily cumulative energy |
| 12 | QSE_var_cum | Quadratic SampEn of sliding variance of daily cumulative energy |

The calculated 12 entropy features are shown in Table 3. As an example, Fig. 7 provides a comparison of the daily maximum energy sequence and the SampEn of its envelope. The abscissa represents the date by serial number (300 days' data given here as an example). The upper and lower half of Fig. 7 represents the maximum energy sequence and the SampEn of its envelope, respectively, while the red vertical line marks the high energy tremor. As shown in Fig. 7, the SampEn sequence basically presents the same platform on the high energy tremor. Fig. 8 shows a comparison of the daily maximum energy sequence and the quadratic SampEn of its envelope. The abscissa represents the date by serial number (300 days' data are given as an example here). The upper part of Fig. 8 presents the maximum energy sequence, and the lower half is the quadratic SampEn of its envelope. The red vertical line marks the high energy tremor. As demonstrated in Fig. 8, the high energy tremor mostly occurs at the rising vertex in the quadratic SampEn sequence. The results of Fig. 7 and 8 show that the MS energy data have significant characteristics in the entropy feature domain before high energy tremors, suggesting these remarkable features can be potentially used for the prediction of high energy tremors.

3) TIME-FREQUENCY DOMAIN FEATURES OF MS ENERGY DATA (2 × 3 × 2 = 12 FEATURES)

Short-time Fourier transform (STFT) and its improved algorithm S transform (ST) are two important methods used for

time-frequency domain analysis [47]–[49]. The STFT and ST of the envelope, sliding average and sliding variance sequence of the daily maximum energy sequence and daily total energy sequence involved in Section 3.1.2, are calculated as features in this section. Details of STFT and ST can be found in the research of Livanos *et al.* [50].

TABLE 4. Overview of the time-frequency domain features of MS energy data.

| Feature index | Feature name | Physical meaning |
|---------------|--------------|---|
| 1 | STFT_env_max | STFT of envelope of daily maximum energy |
| 2 | ST_env_max | ST of envelope of daily maximum energy |
| 3 | STFT_ave_max | STFT of sliding average of daily maximum energy |
| 4 | ST_ave_max | ST of sliding average of daily maximum energy |
| 5 | STFT_var_max | STFT of sliding variance of daily maximum energy |
| 6 | ST_var_max | ST of sliding variance of daily maximum energy |
| 7 | STFT_env_cum | STFT of envelope of daily cumulative energy |
| 8 | ST_env_cum | ST of envelope of daily cumulative energy |
| 9 | STFT_ave_cum | STFT of sliding average of daily cumulative energy |
| 10 | ST_ave_cum | ST of sliding average of daily cumulative energy |
| 11 | STFT_var_cum | STFT of sliding variance of daily cumulative energy |
| 12 | ST_var_cum | ST of sliding variance of daily cumulative energy |

The calculated 12 time-frequency domain features are listed in Table 4. As an example, Fig. 9 shows a comparison of the daily maximum energy sequence and the STFT of its envelope. The upper half of Fig. 9 presents the daily maximum energy sequence, while the lower half presents STFT of its envelope. The red vertical line marks the high energy tremor. As indicated in Fig. 9, the high energy tremor is at or near the rising vertex in the STFT sequence. Fig. 10 illustrates the daily maximum energy sequence and ST of its envelope. The upper half of Fig. 10 presents the daily maximum energy sequence, while the lower half shows the ST of its envelope. The red vertical line marks the high energy tremor. As demonstrated in Fig. 10, the slope of the curve basically begins to decrease from the occurrence of high energy tremor in ST sequence. The results of Fig. 9 and 10 show that MS energy data have significant characteristics in the time-frequency domain before the high energy tremor occurs. These remarkable features can be used for predicting high energy tremors potentially.

4) SUMMARY

In this section, a total of 156 features are extracted in three feature domains. As discussed above, these features demonstrate obvious characteristics before the high energy

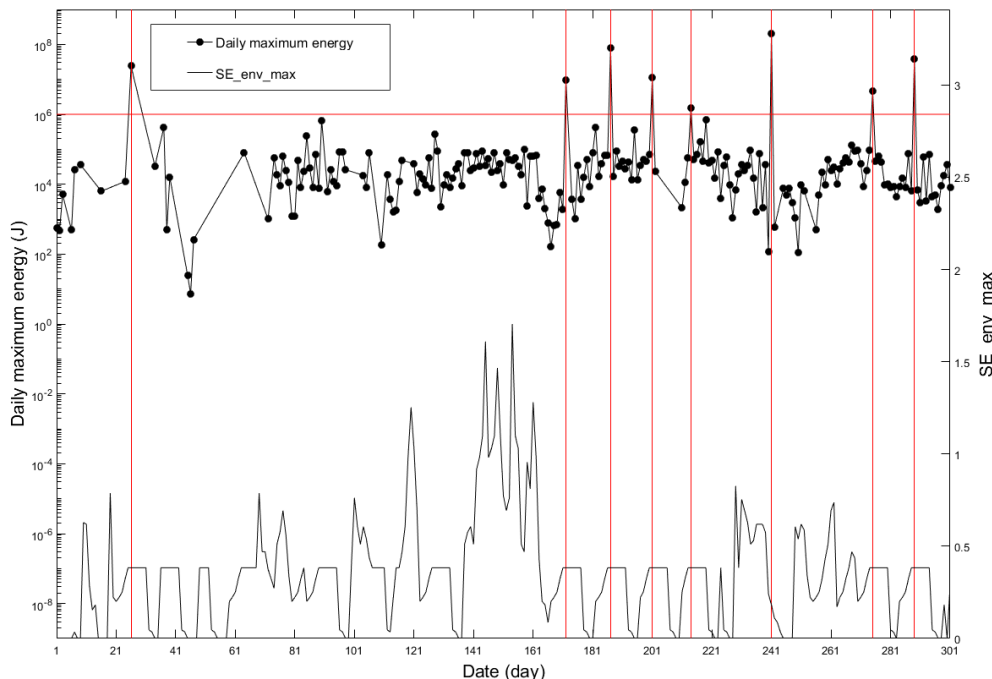


FIGURE 7. Comparison of the daily maximum energy sequence and the SampEn of its envelope.

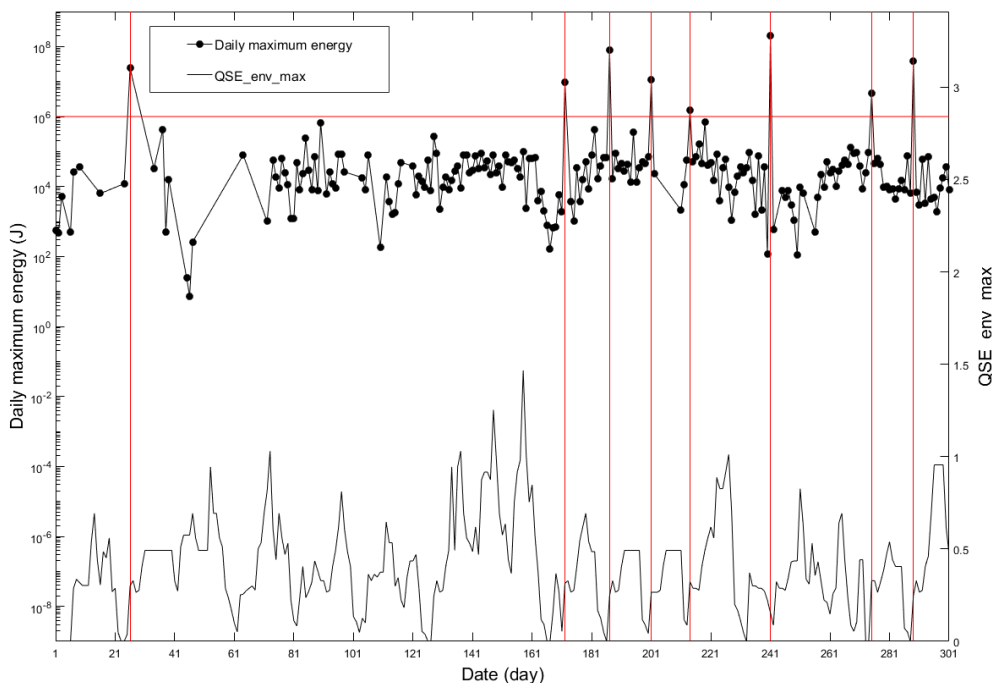


FIGURE 8. Comparison of the daily maximum energy sequence and the quadratic SampEn of its envelope.

tremor occurs, having potentials to be used for high energy tremor prediction. A brief overview of these features is shown in Table 5. According to author’s knowledge, existing studies rarely extract so many multidimensional features from MS raw wave and energy data. Therefore, extracting these potential features in three domains serves as an important novelty of this study.

B. FEATURE SELECTION AND HYPERPARAMETERS OPTIMIZATION BASED ON GA

Feature selection refers to picking up appropriate and efficient ones from the potential features extracted above. In addition, four unknown hyperparameters of SVM model, including c , g , w_1 and w_0 , need to be determined (details of these hyperparameters included in Section 3.3). GA is

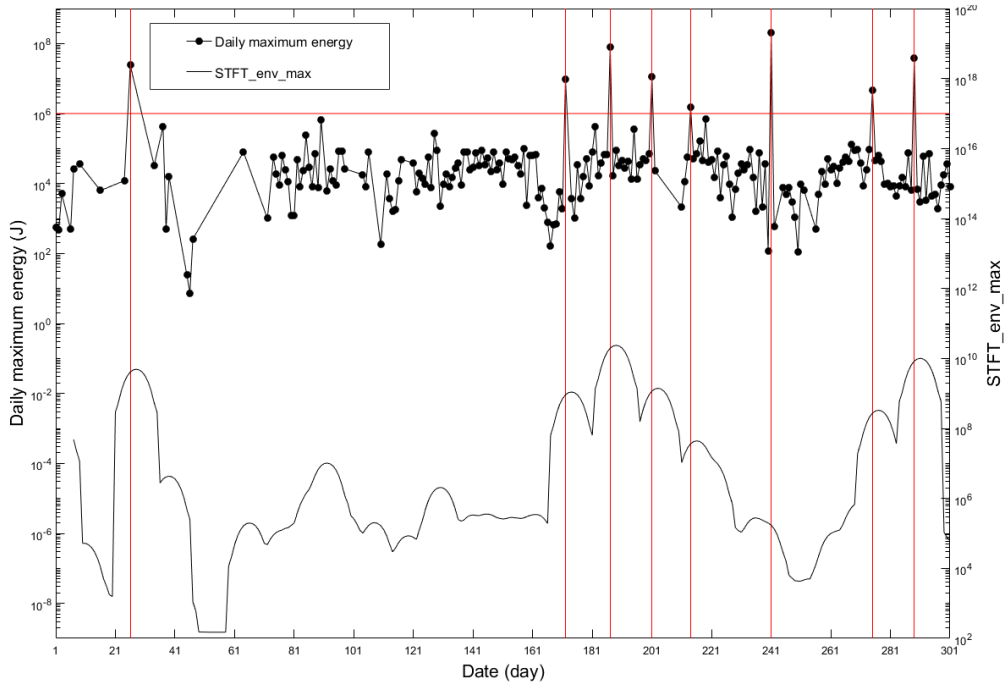


FIGURE 9. Comparison of the daily maximum energy sequence and the STFT of its envelope.

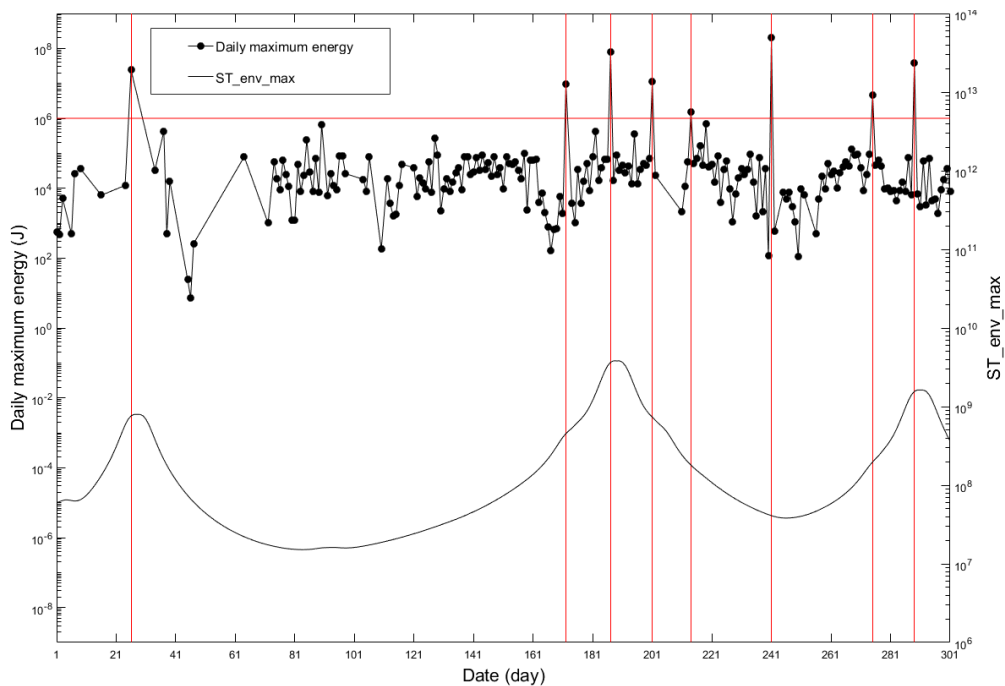


FIGURE 10. Comparison of the daily maximum energy sequence and the ST of its envelope.

utilized in the paper to perform feature selection and parameter optimization of SVM simultaneously. GA is achieved following such steps: perform the recombination and mutation of the population at first, then merge populations, and finally perform the selection operation based on fitness function to maximize the possible optimal individuals.

The chromosomal coding of the initial population includes feature selection portion and parameter optimization portion, and each gene of the chromosome uses a binary code. The feature selection part includes 156 bits, corresponding to 156 features. If the value of the gene is “1”, the corresponding feature is selected. Otherwise, a value of “0” indicates that the corresponding feature is not selected. The parameter

TABLE 5. Overview of the features extracted in this paper.

| Index | Domain | Number of features | Motivation |
|-------|---|--------------------|---|
| 1 | Entropy | 12 | Reflect the MS energy data complexity. |
| 2 | Time-frequency domain | 12 | Extract time-frequency features of the MS energy data. |
| 3 | Statistics features based on frequency domain | 132 | Extract statistical features based on frequency domain of the MS raw wave data. |
| Total | -- | 156 | -- |

optimization part includes 32 bits, including c , g , w_1 and w_0 . The initial 156-bit code is generated in a random manner as the initial population. A multi-point crossover method was used for recombination, considering long chromosomes [51], [52]. The number of mutant chromosomes was determined by the present mutation rate, and their values were changed from “1” to “0” or “0” to “1”. The fitness function is used to evaluate the performance of individuals in a population, and determine the individuals suitable for the best solution. After the mutation operation, the parent population and the sub-population were combined, and then the fitness of the newly combined population was evaluated. Ten-fold cross validation is performed in this work.

C. SVM MODEL CONSTRUCTION

Radial basis function (RBF) is one of the most popular kernel functions for nonlinear problems [53], and is chosen for SVM. There are four hyperparameters for SVM, c , g , w_1 and w_0 . c is a regularization parameter between complexity and classification accuracy; g is a parameter of RBF; w_1 and w_0 are the punish coefficients of high energy tremors and general MS events, respectively. These four hyperparameters are simultaneously optimized by GA as discussed in Section 3.2. Multiple indicators are established to assess prediction accuracy, including accuracy, sensitivity and specificity. These parameters are calculated following Eqs. (1)-(3).

$$Acc_i = \frac{TP_i + TN_i}{TP_i + FP_i + TN_i + FN_i} \quad (1)$$

$$Sens_i = \frac{TP_i}{TP_i + FN_i} \quad (2)$$

$$Spec_i = \frac{TN_i}{FP_i + TN_i} \quad (3)$$

where Acc_i , $Sens_i$ and $Spec_i$ indicate the accuracy, sensitivity and specificity in the i th evaluation, respectively. TP_i , FP_i , TN_i , and FN_i represent the number of true positive, false positive, true negative and false negative results in the i th evaluation, respectively.

IV. RESULTS AND DISCUSSION

Based on the method discussed above, this paper analyses the real MS data collected from Wudong Coal Mine in Xinjiang, China. The code implementation was performed via

the Python 3 language (Anaconda, Anaconda, Inc., Texas, USA). The MS monitoring system used in this experiment installed a total of 12 sensors underground, thereby avoiding the interference of artificial noise as far as possible [54]. The system locates MS events and records signals only when signals are detected by more than four sensors. The interference signals have equal amplitudes, and are automatically filtered by the monitor system. The obtained MS data from the monitor system has a high signal-noise ratio and thereby no additional filter operation is performed in this study. 132 and 24 features are initially extracted from MS raw wave and energy data in frequency domain, entropy and time-frequency domain, respectively. The parameters of GA are determined empirically and their values are listed in Table 6. When MS raw wave and energy data are both used, 83% (55 features) of 66 selected features are from MS raw wave data, while remaining 17% (11 features) from MS energy data. These results indicate that the MS raw wave serves an essential part of MS data, contributing a lot to rockburst risk forecasting [34]–[36]. 63 or 10 features are selected from 132 or 24 extracted features from MS raw wave or energy data, under condition that one kind of data is solely used.

TABLE 6. Parameters of GA.

| Description | Setting |
|---------------------|----------------------------------|
| Population size | 200 |
| Recombine type | Multi-point crossover |
| Recombine rate | 0.9 |
| Mutation rate | 0.1 |
| Selection technique | Elitism and tournament selection |
| Iteration number | 500 |

TABLE 7. Selection results of MS energy features when MS raw wave and energy data were both used.

| Feature index | Feature name |
|---------------|--------------|
| 1 | SE_var_max |
| 2 | QSE_var_max |
| 3 | STFT_var_max |
| 4 | SE_env_cum |
| 5 | QSE_env_cum |
| 6 | STFT_env_cum |
| 7 | SE_ave_cum |
| 8 | STFT_ave_cum |
| 9 | SE_var_cum |
| 10 | STFT_var_cum |
| 11 | ST_var_cum |

As demonstrated in Table 7, eight of eleven effective features from MS energy data are extracted from the daily total energy, indicating that the daily total energy is important for rockburst risk prediction. These findings are consistent with the conclusions of several existing studies [21], [26], [27], and also help to explain why these studies use daily total energy as an analysis factor in these studies. The remaining three features of eleven selected features from MS energy data are extracted from the daily maximum energy. Three features all represent the sliding variance correlation features of the daily maximum energy, suggesting the fluctuation degree of

the daily maximum energy being an effective indicator of rockburst risk prediction as well. As for the extracted features from the MS energy data, the ratio of entropy features to time-frequency domain features is 6:5, which indicates that the entropy features and the time-frequency domain features are both important.

TABLE 8. Hyperparameters and their values in the SVM model.

| | c | g | w1 | w0 |
|---------------|------|----------|---------|--------|
| Both | 2048 | 0.000031 | 53.6508 | 0.3282 |
| Raw wave data | 1024 | 0.000086 | 28.8889 | 0.2871 |
| Energy data | 5.66 | 0.125 | 27.6190 | 0.6475 |

TABLE 9. The best results obtained from the GA-SVM fusion algorithm.

| | Number of raw wave features | Number of energy features | Accuracy (%) | Sensitivity (%) | Specificity (%) |
|---------------|-----------------------------|---------------------------|--------------|-----------------|-----------------|
| Both | 55 | 11 | 88 | 98 | 87 |
| Raw wave data | 63 | -- | 84 | 98 | 83 |
| Energy data | -- | 10 | 86 | 98 | 85 |

The ratio of the training set to test set is 6:4 in SVM model. 10-fold cross-validation is used to verify the prediction results, considering the number of high energy tremors is relatively small. The accuracy, sensitivity and specificity refer to mean values calculated in 10-fold cross-validation experiments. The general criterion to evaluate the prediction efficiency is that whether a high energy tremor or rockburst occurs within five-day period after prediction of danger [55].

Table 9 shows experimental results under three cases. The sensitivity, accuracy and specificity was 98% or 98%, 84% or 86% and 83% or 85%, when MS raw wave or energy data was solely utilized. The performance is best when MS raw wave and energy data were both used. That is: the sensitivity, accuracy and specificity was 98%, 88% and 87%, respectively. This study not only increased the sensitivity of rockburst risk prediction from 87% [41] to 98%, but also achieved 88% accuracy and 87% specificity, which was not achieved in previous studies. Such improvements may attribute to more features extracted from multi-domains and utilizing MS energy as well as raw wave data.

V. CONCLUSION

A rockburst is a severe hazard and can result in serious destruction to equipments and buildings in mining areas. Considering the high energy tremor is likely to induce severe rockburst disasters, its early warning is of great significance to rockburst risk prediction. MS monitoring has been demonstrated to be a feasible way to forecast rockburst. In this context, contribution of MS raw wave and energy data to rockburst risk prediction was investigated based on a GA-SVM approach. GA is used to select the effective ones from initially extracted features from MS raw wave and energy data, and optimize the hyperparameters of the SVM model. As demon-

strated in research results, the predication performance is better based on both MS raw wave and energy data, comparing to solely utilizing MS raw wave or energy data. Additionally, 83% of all selected features are from MS raw wave data, with the remaining 17% from MS energy data, in case that MS raw wave and energy data are both used. Hence it can be concluded that MS raw wave data serves as an important part of MS data, and should not be neglected in rockburst risk prediction. Rockburst occurs very rarely and the limited amount of high energy tremors was collected in the present study, although over 400 days' MS data were obtained in Wudong Coal Mine. Therefore the performance of the proposed method requires the further verification based on more real data from the coal mine. This serves a limitation of this paper.

APPENDIX

Definition of quadratic SampEn

Suppose A, B and C are time series, respectively.

Suppose $y = \text{SampEn}(x)$ represents a function to calculate the SampEn of x.

Then,

$B = \text{SampEn}(A)$

$C = \text{SampEn}(B)$

C represents the quadratic SampEn of A.

CONFLICT OF INTEREST

The authors declare that they have no conflict of interest.

REFERENCES

- [1] G. Bräuner, *Rockbursts in Coal Mines and Their Prevention*. Evanston, IL, USA: Routledge, 2017.
- [2] S. J. Gibowicz and A. Kijko, *An Introduction to Mining Seismology*, vol. 55. Amsterdam, The Netherlands: Elsevier, 2013.
- [3] C. Anye, "Research on seismic effort of burst and failure of coal rock mass associated with mining and its application," *J. China Coal Soc.*, vol. 36, no. 1, pp. 177–178, 2011.
- [4] W. E. Heinrichs, Jr., R. C. Holmer, R. E. MacDougall, G. R. Rogers, J. S. Sumner, and S. H. Ward, *Mining Geophysics, Theory*, vol. 2. Tulsa, OK, USA: Society of Exploration Geophysicists, 1967.
- [5] M. Cai, "Principles of rock support in burst-prone ground," *Tunnelling Underground Space Technol.*, vol. 36, pp. 46–56, Jun. 2013.
- [6] J. Calleja and J. Nemicik, "Coalburst causes and mechanisms," in *Proc. Coal Oper. Conf.* Wollongong, NSW, Australia: Univ. of Wollongong, Feb. 2016, pp. 310–320.
- [7] Mkaqw. (2018). Coal mine accident analysis. Coal Mine Safety. Accessed: Jan. 16, 2019. [Online]. Available: <http://www.mkaqw.org/html/2018/09/12/460909.shtml>
- [8] Swa. (2019). Fatality statistics by industry. Safe Work Australia. Accessed: Jan. 16, 2019. [Online]. Available: <https://www.sa.gov.au/statistics-and-research/statistics/fatalities/fatality-statistics-industry>
- [9] Msha. (2019). Coal Fatalities for 1900 Through 2018. Mine Safety and Health Administration. Accessed: Jan. 18, 2019. [Online]. Available: <https://arlweb.msha.gov/stats/centurystats/coalstats.asp>
- [10] AIT. (2018). Investigation report on the '11·11' serious roof accident of Hongyang no. 3 coal mine. Shenyang Coking Coal. Accessed: Jan. 18, 2019. [Online]. Available: <http://www.chinacoal-safety.gov.cn/gk/sgcc/sbg/201812/P020181220624643725275.pdf>
- [11] MEM. (2018). Serious production safety accident. Ministry of Emergency Management of the People's Republic of China. Accessed: Jan. 18, 2019. [Online]. Available: http://www.chinasafety.gov.cn/gk/jsts/201811/t20181116_222139.shtml
- [12] H. He, L. Dou, S. Gong, P. Zhou, Z. Xue, and J. He, "Study of acoustic emission monitoring technology for rockburst," *Rock Soil Mech.*, vol. 32, no. 4, pp. 1262–1268, 2011.

- [13] E. Wang, X. He, J. Wei, B. Nie, and D. Song, "Electromagnetic emission graded warning model and its applications against coal rock dynamic collapses," *Int. J. Rock Mech. Mining Sci.*, vol. 48, no. 4, pp. 556–564, Jun. 2011.
- [14] S.-T. Gu, C.-Q. Wang, B.-Y. Jiang, Y.-L. Tan, and N.-N. Li, "Field test of rock burst danger based on drilling pulverized coal parameters," *Disaster Adv.*, vol. 5, no. 4, pp. 237–240, 2012.
- [15] Y. Zhou and T. Wang, "PNN-based rockburst prediction model and its applications," *Earth Sci. Res. J.*, vol. 21, no. 3, pp. 141–146, 2017.
- [16] J. Chen, Y. Chen, S. Yang, X. Zhong, and X. Han, "A prediction model on rockburst intensity grade based on variable weight and matter-element extension," *PLoS ONE*, vol. 14, no. 6, 2019, Art. no. e0218525.
- [17] B. Jiang, L. Wang, Y. Lu, C. Wang, and D. Ma, "Combined early warning method for rockburst in a Deep Island, fully mechanized caving face," *Arabian J. Geosci.*, vol. 9, no. 20, p. 743, Dec. 2016.
- [18] S. Zhu, Y. Feng, F. Jiang, and J. Liu, "Mechanism and risk assessment of overall-instability-induced rockbursts in deep island longwall panels," *Int. J. Rock Mech. Mining Sci.*, vol. 106, pp. 342–349, Jun. 2018.
- [19] D. Song, E. Wang, Z. Li, L. Qiu, and Z. Xu, "EMR: An effective method for monitoring and warning of rock burst hazard," *Geomechanics Eng.*, vol. 12, no. 1, pp. 53–69, Jan. 2017.
- [20] G. Su, Y. Shi, X. Feng, J. Jiang, J. Zhang, and Q. Jiang, "True-triaxial experimental study of the evolutionary features of the acoustic emissions and sounds of rockburst processes," *Rock Mech. Rock Eng.*, vol. 51, no. 2, pp. 375–389, Feb. 2018.
- [21] S. He, D. Song, Z. Li, X. He, J. Chen, D. Li, and X. Tian, "Precursor of spatio-temporal evolution law of MS and AE activities for rock burst warning in steeply inclined and extremely thick coal seams under caving mining conditions," *Rock Mech. Rock Eng.*, vol. 52, no. 7, pp. 2415–2435, Jul. 2019.
- [22] M. Cai, P. K. Kaiser, H. Morioka, M. Minami, T. Maejima, Y. Tasaka, and H. Kurose, "FLAC/PFC coupled numerical simulation of AE in large-scale underground excavations," *Int. J. Rock Mech. Mining Sci.*, vol. 44, no. 4, pp. 550–564, Jun. 2007.
- [23] K. Sato, T. Isobe, N. Mori, and T. Goto, "Microseismic activity associated with hydraulic mining," *Int. J. Rock Mech. Mining Sci. Geomechanics Abstr.*, vol. 23, no. 1, pp. 85–94, 1986.
- [24] F. Leighton, *A Case History of a Major Rock Burst*. Washington, DC, USA: US Department of the Interior, Bureau of Mines, 1982.
- [25] S. Wang, C. Li, W. Yan, Z. Zou, and W. Chen, "Multiple indicators prediction method of rock burst based on microseismic monitoring technology," *Arabian J. Geosci.*, vol. 10, no. 6, p. 132, Mar. 2017.
- [26] C.-P. Lu, G.-J. Liu, Y. Liu, N. Zhang, J.-H. Xue, and L. Zhang, "Microseismic multi-parameter characteristics of rockburst hazard induced by hard roof fall and high stress concentration," *Int. J. Rock Mech. Mining Sci.*, vol. 76, pp. 18–32, Jun. 2015.
- [27] Z.-L. Li, X.-Q. He, L.-M. Dou, and G.-F. Wang, "Rockburst occurrences and microseismicity in a longwall panel experiencing frequent rockbursts," *Geosci. J.*, vol. 22, no. 4, pp. 623–639, Aug. 2018.
- [28] A.-Y. Cao, L.-M. Dou, C.-B. Wang, X.-X. Yao, J.-Y. Dong, and Y. Gu, "Microseismic precursory characteristics of rock burst hazard in mining areas near a large residual coal pillar: A case study from Xuzhuang coal mine, Xuzhou, China," *Rock Mech. Rock Eng.*, vol. 49, no. 11, pp. 4407–4422, Nov. 2016.
- [29] F.-X. Jiang, S.-H. Yang, Y.-H. Cheng, X.-M. Zhang, Z. Mao, and F. Xu, "A study on microseismic monitoring of rock burst in coal mine," *Chin. J. Geophys.*, vol. 49, no. 5, pp. 1511–1516, 2006.
- [30] A. Leśniak and Z. Isakow, "Space-time clustering of seismic events and hazard assessment in the zabrze-Bielszowice coal mine, Poland," *Int. J. Rock Mech. Mining Sci.*, vol. 46, no. 5, pp. 918–928, Jul. 2009.
- [31] Y.-X. Zhao, Y.-D. Jiang, T. Wang, F. Gao, and S.-T. Xie, "Features of microseismic events and precursors of rock burst in underground coal mining with hard roof," *J. China Coal Soc.*, vol. 37, no. 12, pp. 1960–1966, 2012.
- [32] Y. Qun, T. Chun-An, and L. Lian-chong, "Nucleation process of rockbursts based on microseismic monitoring of deep-buried tunnels for Jinping 2 hydropower station," *Chin. J. Geotech. Eng.*, vol. 36, no. 12, pp. 2315–2322, 2014.
- [33] P. Jha and R. Chouhan, "Long range rockburst prediction: A seismological approach," *Int. J. Rock Mech. Mining Sci. Geomechanics Abstr.*, vol. 31, no. 1, pp. 71–77, 1994.
- [34] A. Lurka and P. Swanson, "Improvements in seismic event locations in a deep Western US coal mine using tomographic velocity models and an evolutionary search algorithm," *Mining Sci. Technol. (China)*, vol. 19, no. 5, pp. 599–603, Sep. 2009.
- [35] A.-Y. Cao, L.-M. Dou, X. Luo, Y.-D. Zheng, J.-L. Huang, and K. Andrew, "Seismic effort of blasting wave transmitted in coal-rock mass associated with mining operation," *J. Central South Univ.*, vol. 19, no. 9, pp. 2604–2610, Sep. 2012.
- [36] C.-P. Lu, Y. Liu, H.-Y. Wang, and P.-F. Liu, "Microseismic signals of double-layer hard and thick igneous strata separation and fracturing," *Int. J. Coal Geol.*, vols. 160–161, pp. 28–41, Apr. 2016.
- [37] V. A. Mansurov, "Prediction of rockbursts by analysis of induced seismicity data," *Int. J. Rock Mech. Mining Sci.*, vol. 38, no. 6, pp. 893–901, Sep. 2001.
- [38] L. Dou, T. Chen, S. Gong, H. He, and S. Zhang, "Rockburst hazard determination by using computed tomography technology in deep workplace," *Saf. Sci.*, vol. 50, no. 4, pp. 736–740, Apr. 2012.
- [39] G.-L. Feng, X.-T. Feng, B.-R. Chen, Y.-X. Xiao, and Y. Yu, "A microseismic method for dynamic warning of rockburst development processes in tunnels," *Rock Mech. Rock Eng.*, vol. 48, no. 5, pp. 2061–2076, Sep. 2015.
- [40] M. Tianhui, T. Chunan, and T. Liexian, "Mechanism of rock burst forecasting based on micro-seismic monitoring technology," *Chin. J. Rock Mech. Eng.*, vol. 35, no. 3, pp. 470–483, 2016.
- [41] G. Feng, G. Xia, B. Chen, Y. Xiao, and R. Zhou, "A method for rockburst prediction in the deep tunnels of hydropower stations based on the monitored microseismicity and an optimized probabilistic neural network model," *Sustainability*, vol. 11, no. 11, p. 3212, 2019.
- [42] V. Vapnik, *The Nature of Statistical Learning Theory*. New York, NY, USA: Springer, 2013.
- [43] J. Shawe-Taylor, P. L. Bartlett, R. C. Williamson, and M. Anthony, "Structural risk minimization over data-dependent hierarchies," *IEEE Trans. Inf. Theory*, vol. 44, no. 5, pp. 1926–1940, Sep. 1998.
- [44] T. Evgeniou and M. Pontil, "Support vector machines: Theory and applications," in *Advanced Course on Artificial Intelligence*. Berlin, Germany: Springer, 1999, pp. 249–257.
- [45] R. Zi-Wu and S. Ye, "Improved adaptive genetic algorithm and its application research in parameter identification," *J. Syst. Simul.*, vol. 18, no. 1, pp. 41–43, 2006.
- [46] L. Zhao, S. Wei, C. Zhang, Y. Zhang, X. Jiang, F. Liu, and C. Liu, "Determination of sample entropy and fuzzy measure entropy parameters for distinguishing congestive heart failure from normal sinus rhythm subjects," *Entropy*, vol. 17, no. 12, pp. 6270–6288, 2015.
- [47] H. Gao, L. Liang, X. Chen, and G. Xu, "Feature extraction and recognition for rolling element bearing fault utilizing short-time Fourier transform and non-negative matrix factorization," *Chin. J. Mech. Eng.*, vol. 28, no. 1, pp. 96–105, Jan. 2015.
- [48] Z.-L. Huang, J. Zhang, T.-H. Zhao, and Y. Sun, "Synchrosqueezing S-transform and its application in seismic spectral decomposition," *IEEE Trans. Geosci. Remote Sens.*, vol. 54, no. 2, pp. 817–825, Feb. 2016.
- [49] S. Mukhopadhyay, N. Ghosh, R. Barman, P. K. Panigrahi, S. Pratihier, and A. Pradhan, "S-transform based fluctuation analysis—A method for pre-cancer detection," in *Proc. Int. Conf. Microelectron., Comput. Commun. (MicroCom)*, Jan. 2016, pp. 1–5.
- [50] G. Livanos, N. Ranganathan, and J. Jiang, "Heart sound analysis using the S transform," in *Proc. Comput. Cardiol.*, vol. 27, 2000, pp. 587–590.
- [51] H. Uğuz, "A two-stage feature selection method for text categorization by using information gain, principal component analysis and genetic algorithm," *Knowl.-Based Syst.*, vol. 24, no. 7, pp. 1024–1032, Oct. 2011.
- [52] A. S. Ghareb, A. A. Bakar, and A. R. Hamdan, "Hybrid feature selection based on enhanced genetic algorithm for text categorization," *Expert Syst. Appl.*, vol. 49, pp. 31–47, May 2016.
- [53] H. Uğuz, "A hybrid system based on information gain and principal component analysis for the classification of transcranial Doppler signals," *Comput. Methods Programs Biomed.*, vol. 107, no. 3, pp. 598–609, Sep. 2012.
- [54] C.-P. Lu, G.-J. Liu, N. Zhang, T.-B. Zhao, and Y. Liu, "Inversion of stress field evolution consisting of static and dynamic stresses by microseismic velocity tomography," *Int. J. Rock Mech. Mining Sci.*, vol. 87, pp. 8–22, Sep. 2016.
- [55] Y. Xia, H. Lan, and X.-Z. Wei, "Study of comprehensive evaluation technology for rock burst hazard based on microseismic and underground sound monitoring," *J. China Coal Soc.*, vol. 36, no. S2, pp. 358–364, 2011.
- [56] S. He, D. Song, X. He, J. Chen, T. Ren, Z. Li, and L. Qiu, "Coupled mechanism of compression and prying-induced rock burst in steeply inclined coal seams and principles for its prevention," *Tunnelling Underground Space Technol.*, vol. 98, Apr. 2020, Art. no. 103327.



BING JI received the bachelor's and master's degrees in electronic engineering from Xidian University, China, in 2007 and 2009, respectively, and the Ph.D. degree in medical engineering from the University of Hull, U.K., in 2012. Since 2012, he has been a Lecturer with Shandong University, China. His research interests include robotic learning, bionic robotics, computational modeling of biological systems, and machine learning.



SHENQUAN HE received the B.S. degree in safety engineering from the China University of Geosciences, in 2015, and the M.S. and Ph.D. degrees from the University of Science and Technology Beijing. His research area is coal and rock dynamic disasters.



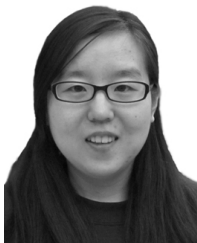
FA XIE received the B.E. degree in process equipment and control engineering from the Beijing Institute of Technology, China. He is currently pursuing the M.E. degree with Shandong University. His current research area is machine learning.



DAZHAO SONG was born in Shandong, China, in 1985. He received the B.S. degree in mining engineering from the Zhongyuan University of Technology, China, in 2007, and the Ph.D. degree in safety technology and engineering from the China University of Mining and Technology, China, in 2012.

From 2012 to 2016, he was a Lecturer and an Associate Professor with the China University of Mining and Technology. Since 2016, he has been a Faculty Member as an Associate Professor with the Department of Safety Science and Engineering, University of Science and Technology Beijing. He is the author of two books, more than 80 articles, and more than 20 patents. His research interests include monitoring and warning physical method of underground engineering dynamic disaster, theory and technology of safety rheology-mutation, and AI theory and technology of underground engineering safety.

Dr. Song has also been the Secretary General and a member of the International Committee on Mine Safety Science and Engineering, since 2018. He was a recipient of the China Occupational Safety and the Health Association Science and Technology Award, in 2017. He was awarded the Beijing Science and Technology Nova by the Beijing Science and Technology Commission, China, in 2018.



XINPEI WANG received the B.S. and Ph.D. degrees in biomedical engineering from Shandong University, Jinan, China, in 2005 and 2011, respectively.

She is currently a Lecturer with the School of Control Science and Engineering, Shandong University. Her current research interests include biomedical signal and image processing, biomedical measurements and devices, and machine learning.

...